Civil Engineering and Applied Solutions

Research Article

journal homepage: ceas.journals.umz.ac.ir

CEAS Civil Engineering and Applied Solutions

Developing Inelastic Jerk Spectra for Pulse-Like Earthquakes

Alireza Garakaninezhad [a*], Saeed Amiri [b]

[a] *Department of Civil Engineering, Faculty of Engineering, University of Jiroft, Jiroft, Kerman, Iran*
[b] *Department of Civil Engineering, Geological and Mining Engineering, Polytechnique Montreal, Montreal, QC, Canada*

ARTICLE INFO

Keywords:
Jerk spectra
Inelastic systems
Pulse-like earthquakes
Strength reduction factor

Article history:
Received 06 October 2025
Accepted 24 October 2025
Available online 01 February 2026

ABSTRACT

Jerk, or jolt, is defined as the time derivative of acceleration. This study investigates the jerk response of inelastic single-degree-of-freedom (SDOF) systems subjected to pulse-like near-fault ground motions. Compared with ordinary non–pulse-like records, pulse-like motions can impose significantly higher demands on structures. In this work, constant-strength spectra for the jerk response of inelastic SDOF systems are developed using a set of 91 pulse-like earthquakes. The influence of key structural parameters, including strength reduction factor, hysteretic behavior, and viscous damping ratio, is examined. The results show that jerk demands exhibit slightly higher sensitivity to viscous damping in the short, normalized period region than in the long-period region. Furthermore, an analytical equation is proposed to estimate jerk demand as a function of the ratio of elastic vibration period to pulse period and the strength reduction factor, for various hysteretic models and damping ratios.

1. Introduction

Jerk, also referred to as jolt, is defined as the time derivative of acceleration, i.e., the rate at which acceleration changes over time. This parameter has been widely applied across various fields [1], such as a design factor in ride comfort evaluation, e.g., in lifts/elevators [2], amusement rides [3-8], buses [9], and ships [10-12]. Jerk has also been examined in the fields of vibration and seismic control, as well as seismic response [13-18]. Tong et al. [16] investigated the fundamental characteristics of acceleration derivatives using ground motions from the 1999 Chi-Chi earthquake (Mw 7.6) and one of its aftershocks (Mw 6.2). He et al. [18] assessed jerk characteristics through elastic and inelastic jerk response spectra and examined the influence of site type, reduction factor, and ductility on these spectra. Taushanov [15] developed and presented relationships and corresponding graphs for the jerk response spectra. Moreover, in another study, Papandreou and Papagiannopoulos [17] examined the overall characteristics of jerk spectra using bilinear SDOF systems, focusing on hysteretic behavior, viscous damping ratio, and yield strength. An equation was also proposed to estimate the jerk demand of such inelastic systems. Yaseen et al. [19] explored the applicability of jerk as a ground motion intensity measure through nonlinear time-history analyses of representative reinforced concrete frame buildings under seismic excitations. Wakui et al. [20] introduced a method to predict plastic deformation in an SDOF system by employing jerk and snap. Snap refers to the second time derivative of acceleration. Additionally, Vukobratović and Ruggieri [21] conducted an extensive review of research focused on jerk in earthquake engineering. Despite the aforementioned research, no prior studies have examined the assessment of jerk demand under pulse-like ground motions. Moreover, comparable to earlier investigations focusing on multiple earthquake events, such as [22-27], future studies may aim to develop inelastic spectra that capture jerk response under these earthquake scenarios.

Near-fault ground motions with pulse-like characteristics can cause severe structural damage. In such earthquakes, when fault rupture propagates toward the site at a velocity close to the shear wave velocity of the soil, a substantial amount of seismic energy may be concentrated into a large pulse of motion, which is typically observable in the velocity time history [28-31], resulting in more severe structural damage compared to far-field earthquakes. A key parameter of near-fault pulse-like ground motions, the

* Corresponding author.
E-mail addresses: a.garakani@ujiroft.ac.ir (A. Garakaninezhad).

https://doi.org/10.22080/ceas.2025.30227.1049
ISSN: 3092-7749/
How to cite this article: Garakaninezhad, A., Amiri, S. Finite Developing Inelastic Jerk Spectra for Pulse-Like Earthquakes. Civil Engineering and Applied Solutions. 2026; 2(2): 85-97. doi:10.22080/ceas.2025.30227.1049.

pulse period (T_p), has a significant impact on the dynamic behavior of structures [32-35]. T_p corresponds to the dominant velocity pulse period extracted using the Baker wavelet-based algorithm [36]. Extensive research has focused on formulating inelastic spectra under pulse-like ground motions, especially with respect to the inelastic displacement ratio [33, 37, 38], residual displacement ratio [39, 40], and inelastic acceleration ratio [41]. Despite these efforts, jerk-based spectra for pulse-like ground motions remain largely unexplored.

Cited previous studies indicate that there is a potential connection between jerk and damage accumulation, fatigue-sensitive components, and seismic control device triggering. High jerk values correspond to rapid acceleration reversals, which can induce additional force spikes in acceleration-sensitive non-structural components and energy dissipation devices. This establishes a performance-based relevance for jerk spectra. Therefore, this study seeks to develop inelastic jerk response spectra using a constant-strength framework, considering the role of the vibration period normalized to the earthquake pulse period (T/T_p), strength reduction factor (R), hysteretic rule, and damping ratio (ξ). Additionally, an analytical equation is proposed to predict the jerk demand based on T/T_p and R for two different hysteretic models and various values of ξ.

2. Structure

In this study, constant-strength spectra are developed in terms of the jerk response under a set of pulse-like earthquakes. A wide range of elastic vibration period normalized by the pulse period (T/T_p), strength reduction factor, and viscous damping ratio is considered as described in Table 1.

Table 1. Structural parameters considered in numerical analyses.

Parameter	Range of parameters
Normalized elastic vibration period (T/T_p)	0.1–3.0 with an increment of 0.1
Strength reduction factor (R)	2.0-6.0 with an increment of 1.0
Viscous damping ratio (ξ)	0.05-0.2 with an increment of 0.05

Additionally, two hysteretic models are used: the linear elastic-perfectly plastic (PP) model and the deteriorating pinching (DP) model, as indicated in Fig. 1. The parameters considered for these models are illustrated in Table 2.

Table 2. Structural parameters.

Parameter	Symbol
K_e	Initial stiffness
u_y	Yield displacement
α	Postyield stiffness ratio
α_c	Degrading stiffness ratio
F_m	Maximum strength
u_m	Displacement value at the maximum strength
$\mu = u_m/u_y$	Displacement ductility ratio
β	Power to specify the degraded degree of the unloading stiffness based on μ
pinch$X$	Pinching factor for the displacement
pinch$Y$	Pinching factor for the strength
damage$_1$	Accumulated damage factor capturing the damage due to the ductility
damage$_2$	Accumulated damage factor capturing the damage due to the energy dissipation

It is noted that the postyield stiffness ratio, α, is assumed to be zero, and the superscripts + and − imply the tension and compression regions, respectively.

Moreover, the values of pinchX and pinchY are set as 0.5, representing moderate pinching effects [42, 43]. Furthermore, a moderate level of 0.05 is considered for damage1 and damage2 [42, 43], and the value of the degraded unloading stiffness factor (β) is zero, as indicated by the default value in [42]. The selected parameters represent moderate deterioration scenarios commonly used in OpenSees calibration examples.

The OpenSees software (Open System for Earthquake Engineering Simulation) [44] is employed to perform dynamic analyses. Additionally, the “Hysteretic material” model [45] which is available in OpenSees, is used to simulate the deteriorating pinching behavior of the SDOF systems.

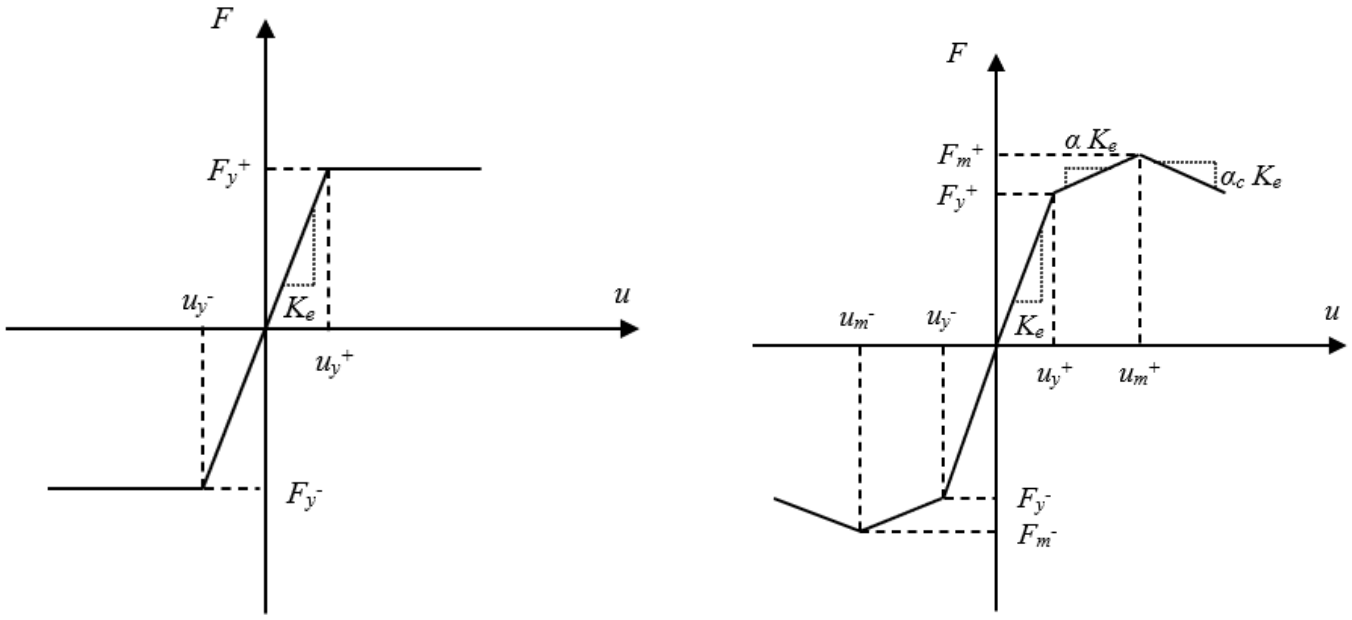

Fig. 1. Hysteretic models: (a) linear elastic-perfectly plastic (PP); and (b) deteriorating pinching (DP).

3. Ground motions

A dataset of pulse-like ground motion, including 91 records identified by Baker [36] is used in this study. These records have been assembled from the Pacific Earthquake Engineering Research (PEER) database [46]. Baker in a study [36] decomposed the original records, then extracted T_p and identified them as pulse-like or non-pulse-like earthquakes using the wavelet transform. Based on the research performed by Baker [36], ground motions could be classified as pulses if the following criteria would be met: (1) The residual ground motion is considerably less intense than the original ground motion, (2) The pulse arrives at the beginning of the time history by measuring the time point when 10% of the pulse energy is observed), (3) The original ground motion that its peak ground velocity (PGV) is higher than 30 cm/s. These criteria are determined by a pulse indicator, which is between 0 and 1. The seismic excitations consist of 23 pulse-like earthquakes, such that their moment magnitude (M_w) is varied from 5 to 7.6. The range of T_P of the earthquakes is from 0.4 s to 12.9 s. Table 3 illustrates the information about these pulse-like earthquakes.

4. Inelastic jerk spectra

4.1. Effect of the strength reduction factor on the inelastic jerk spectra

After conducting nonlinear time history analyses of the SDOF systems under the near-fault pulse-like ground motions, the jerk is derived by differentiating the relative acceleration response of the systems. Then, the mean jerk spectra for different R, ξ, and hysteretic models are presented in this section, such that the horizontal axis of the spectra is T/T_p. The effect of the strength reduction factor on the mean jerk spectra is illustrated in Figs. 2 and 3 for the PP and DP hysteretic rules, respectively. Fig. 2 shows that the impact of R on the jerk response is more pronounced for $T/T_p \leq 1.0$ s, such that decreasing R leads to an increase in the jerk demand. For instance, the mean jerk of the system with the PP hysteretic model, $T/T_p = 0.5$.

Table 3. Pulse-like ground motions.

No.	Event	Year	Station	T_p	PGV	M_w	Epi. distance	Pulse indicator
1	San Fernando	1971	Pacoima Dam (upper left abut)	1.6	116.5	6.6	11.9	0.97
2	Coyote Lake	1979	Gilroy Array #6	1.2	51.5	5.7	4.4	1.00
3	Imperial Valley-06	1979	Aeropuerto Mexicali	2.4	44.3	6.5	2.5	0.99
4	Imperial Valley-06	1979	Agrarias	2.3	54.4	6.5	2.6	1.00
5	Imperial Valley-06	1979	Brawley Airport	4.0	36.1	6.5	43.2	1.00
6	Imperial Valley-06	1979	EC County Center FF	4.5	54.5	6.5	29.1	1.00
7	Imperial Valley-06	1979	EC Meloland Overpass FF	3.3	115.0	6.5	19.4	1.00
8	Imperial Valley-06	1979	El Centro Array #10	4.5	46.9	6.5	26.3	1.00
9	Imperial Valley-06	1979	El Centro Array #11	7.4	41.1	6.5	29.4	0.92
10	Imperial Valley-06	1979	El Centro Array #3	5.2	41.1	6.5	28.7	1.00
11	Imperial Valley-06	1979	El Centro Array #4	4.6	77.9	6.5	27.1	1.00
12	Imperial Valley-06	1979	El Centro Array #5	4.0	91.5	6.5	27.8	1.00
13	Imperial Valley-06	1979	El Centro Array #6	3.8	111.9	6.5	27.5	1.00

14	Imperial Valley-06	1979	El Centro Array #7	4.2	108.8	6.5	27.6	1.00
15	Imperial Valley-06	1979	El Centro Array #8	5.4	48.6	6.5	28.1	1.00
16	Imperial Valley-06	1979	El Centro Differential Array	5.9	59.6	6.5	27.2	1.00
17	Imperial Valley-06	1979	Holtville Post Office	4.8	55.1	6.5	19.8	1.00
18	Mammoth Lakes-06	1980	Long Valley Dam (Upr L Abut)	1.1	33.1	5.9	14.0	1.00
19	Irpinia, Italy-01	1980	Sturno	3.1	41.5	6.9	30.4	0.94
20	Westmorland	1981	Parachute Test Site	3.6	35.8	5.9	20.5	0.89
21	Coalinga-05	1983	Oil City	0.7	41.2	5.8	4.6	0.92
22	Coalinga-05	1983	Transmitter Hill	0.9	46.1	5.8	6.0	0.96
23	Coalinga-07	1983	Coalinga-14th & Elm (Old CHP)	0.4	36.1	5.2	9.6	1.00
24	Morgan Hill	1984	Coyote Lake Dam (SW Abut)	1.0	62.3	6.2	24.6	0.99
25	Morgan Hill	1984	Gilroy Array #6	1.2	35.4	6.2	36.3	1.00
26	Taiwan SMART1(40)	1986	SMART1 C00	1.6	31.2	6.3	68.2	1.00
27	Taiwan SMART1(40)	1986	SMART1 M07	1.6	36.1	6.3	67.2	1.00
28	N. Palm Springs	1986	North Palm Springs	1.4	73.6	6.1	10.6	1.00
29	San Salvador	1986	Geotech Investig Center	0.9	62.3	5.8	7.9	0.99
30	Whittier Narrows-01	1987	Downey - Co Maint Bldg	0.8	30.4	6.0	16.0	1.00
31	Whittier Narrows-01	1987	LB - Orange Ave	1.0	32.9	6.0	20.7	1.00
32	Superstition Hills-02	1987	Parachute Test Site	2.3	106.8	6.5	16.0	1.00
33	Loma Prieta	1989	Alameda Naval Air Stn Hanger	2.0	32.2	6.9	90.8	1.00
34	Loma Prieta	1989	Gilroy Array #2	1.7	45.7	6.9	29.8	0.98
35	Loma Prieta	1989	Oakland - Outer Harbor Wharf	1.8	49.2	6.9	94.0	1.00
36	Loma Prieta	1989	Saratoga - Aloha Ave	4.5	55.6	6.9	27.2	0.86
37	Erzican, Turkey	1992	Erzincan	2.7	95.4	6.7	9.0	1.00
38	Cape Mendocino	1992	Petrolia	3.0	82.1	7.0	4.5	0.92
39	Landers	1992	Barstow	8.9	30.4	7.3	94.8	1.00
40	Landers	1992	Lucerne	5.1	140.3	7.3	44.0	1.00
41	Landers	1992	Yermo Fire Station	7.5	53.2	7.3	86.0	1.00
42	Northridge-01	1994	Jensen Filter Plant	3.5	67.4	6.7	13.0	1.00
43	Northridge-01	1994	Jensen Filter Plant Generator	3.5	67.4	6.7	13.0	1.00
44	Northridge-01	1994	LA - Wadsworth VA Hospital North	2.4	32.4	6.7	19.6	0.96
45	Northridge-01	1994	LA Dam	1.7	77.1	6.7	11.8	1.00
46	Northridge-01	1994	Newhall - W Pico Canyon Rd.	2.4	87.8	6.7	21.6	1.00
47	Northridge-01	1994	Pacoima Dam (downstr)	0.5	50.4	6.7	20.4	0.87
48	Northridge-01	1994	Pacoima Dam (upper left)	0.9	107.1	6.7	20.4	1.00
49	Northridge-01	1994	Rinaldi Receiving Sta	1.2	167.2	6.7	10.9	1.00
50	Northridge-01	1994	Sylmar - Converter Sta	3.5	130.3	6.7	13.1	0.92
51	Northridge-01	1994	Sylmar - Converter Sta East	3.5	116.6	6.7	13.6	1.00
52	Northridge-01	1994	Sylmar - Olive View Med FF	3.1	122.7	6.7	16.8	1.00
53	Kobe, Japan	1995	Takarazuka	1.4	72.6	6.9	38.6	0.87
54	Kobe, Japan	1995	Takatori	1.6	169.6	6.9	13.1	0.96
55	Kocaeli, Turkey	1999	Gebze	5.9	52.0	7.5	47.0	1.00
56	Chi-Chi, Taiwan	1999	CHY006	2.6	64.7	7.6	40.5	0.97
57	Chi-Chi, Taiwan	1999	CHY035	1.4	42.0	7.6	43.9	0.95
58	Chi-Chi, Taiwan	1999	CHY101	4.8	85.4	7.6	32.0	1.00
59	Chi-Chi, Taiwan	1999	TAP003	3.4	33.0	7.6	151.7	0.99
60	Chi-Chi, Taiwan	1999	TCU029	6.4	62.3	7.6	79.2	1.00
61	Chi-Chi, Taiwan	1999	TCU031	6.2	59.9	7.6	80.1	1.00
62	Chi-Chi, Taiwan	1999	TCU034	8.6	42.8	7.6	87.9	1.00
63	Chi-Chi, Taiwan	1999	TCU036	5.4	62.4	7.6	67.8	1.00
64	Chi-Chi, Taiwan	1999	TCU038	7.0	50.9	7.6	73.1	1.00

65	Chi-Chi, Taiwan	1999	TCU040	6.3	53.0	7.6	69.0	1.00
66	Chi-Chi, Taiwan	1999	TCU042	9.1	47.3	7.6	78.4	1.00
67	Chi-Chi, Taiwan	1999	TCU046	8.6	44.0	7.6	68.9	1.00
68	Chi-Chi, Taiwan	1999	TCU049	11.8	44.8	7.6	38.9	0.99
69	Chi-Chi, Taiwan	1999	TCU053	12.9	41.9	7.6	41.2	1.00
70	Chi-Chi, Taiwan	1999	TCU054	10.5	60.9	7.6	37.6	1.00
71	Chi-Chi, Taiwan	1999	TCU056	12.9	43.5	7.6	39.7	0.95
72	Chi-Chi, Taiwan	1999	TCU060	12.0	33.7	7.6	45.4	0.99
73	Chi-Chi, Taiwan	1999	TCU065	5.7	127.7	7.6	26.7	0.96
74	Chi-Chi, Taiwan	1999	TCU068	12.2	191.1	7.6	47.9	1.00
75	Chi-Chi, Taiwan	1999	TCU075	5.1	88.4	7.6	20.7	1.00
76	Chi-Chi, Taiwan	1999	TCU076	4.0	63.7	7.6	16.0	0.92
77	Chi-Chi, Taiwan	1999	TCU082	9.2	56.1	7.6	36.2	0.95
78	Chi-Chi, Taiwan	1999	TCU087	9.0	53.7	7.6	55.6	1.00
79	Chi-Chi, Taiwan	1999	TCU098	7.5	32.7	7.6	99.7	0.97
80	Chi-Chi, Taiwan	1999	TCU101	10.0	68.4	7.6	45.1	1.00
81	Chi-Chi, Taiwan	1999	TCU102	9.7	106.6	7.6	45.6	0.97
82	Chi-Chi, Taiwan	1999	TCU103	8.3	62.2	7.6	52.4	1.00
83	Chi-Chi, Taiwan	1999	TCU104	12.0	31.4	7.6	49.3	0.99
84	Chi-Chi, Taiwan	1999	TCU128	9.0	78.7	7.6	63.3	1.00
85	Chi-Chi, Taiwan	1999	TCU136	10.3	51.8	7.6	48.8	1.00
86	Northwest China-03	1997	Jiashi	1.3	37.0	6.1	19.1	1.00
87	Yountville	2000	Napa Fire Station #3	0.7	43.0	5.0	9.9	1.00
88	Chi-Chi, Taiwan-03	1999	CHY024	3.2	33.1	6.2	25.5	1.00
89	Chi-Chi, Taiwan-03	1999	CHY080	1.4	69.9	6.2	29.5	1.00
90	Chi-Chi, Taiwan-03	1999	TCU076	0.9	59.4	6.2	20.8	1.00
91	Chi-Chi, Taiwan-06	1999	CHY101	2.8	36.3	6.3	50.0	1.00

And $\xi = 0.05$ varies from 26.40 m/s^3 to 35.77 m/s^3, corresponding to an increase of roughly 35.5%, as R decreases from 6 to 2. Additionally, the structures with longer T/T_p values experience lower jerk response than those with shorter T/T_p values. Specifically, within the $2.0 \leq T/T_p \leq 3.0$ s range, the jerk demand stabilizes at an average value of 8.40 m/s^3 for all the considered R values. Moreover, similar trends are observed for the other values of ξ ($\xi = 0.1, 0.15, 0.2$); however, the effect of R on J diminishes in the region of $T/T_p \leq 1.0$ s with increasing ξ, as shown in Fig. 2(c)(e)(g). Based on Fig. 3, the effect of R on the mean jerk of the systems with the DP model and $T/T_p \leq 1.0$ is more significant than in the systems with the PP model. For example, in the system with the DP model, $T/T_p = 0.5$ and $\xi = 0.05$, the jerk changes from 21.18 m/s^3 to 34.48 m/s^3, an increase of approximately 62.80%, when R decreases from 6 to 2.

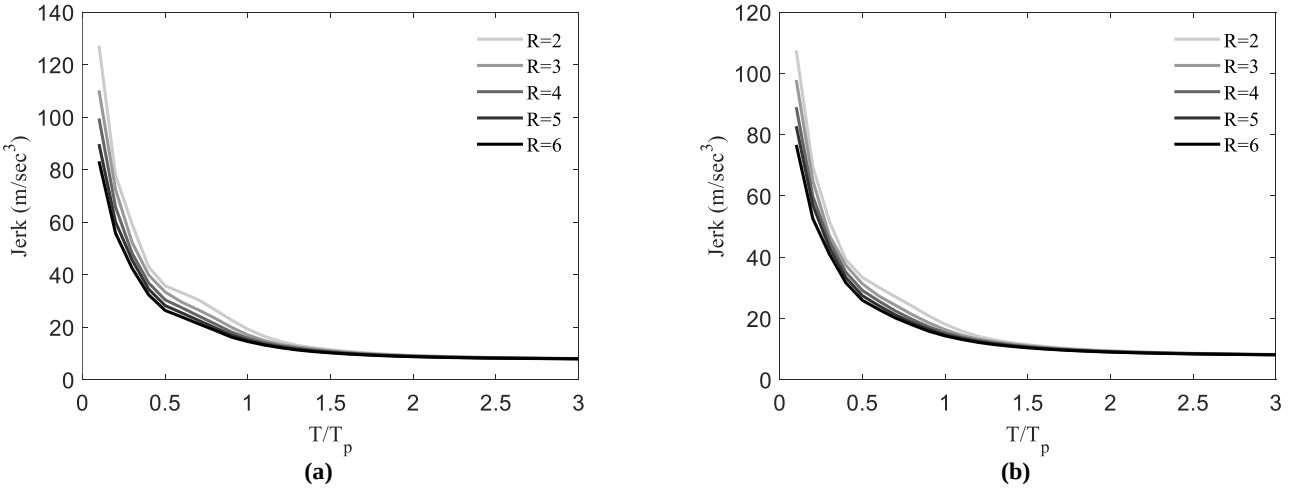

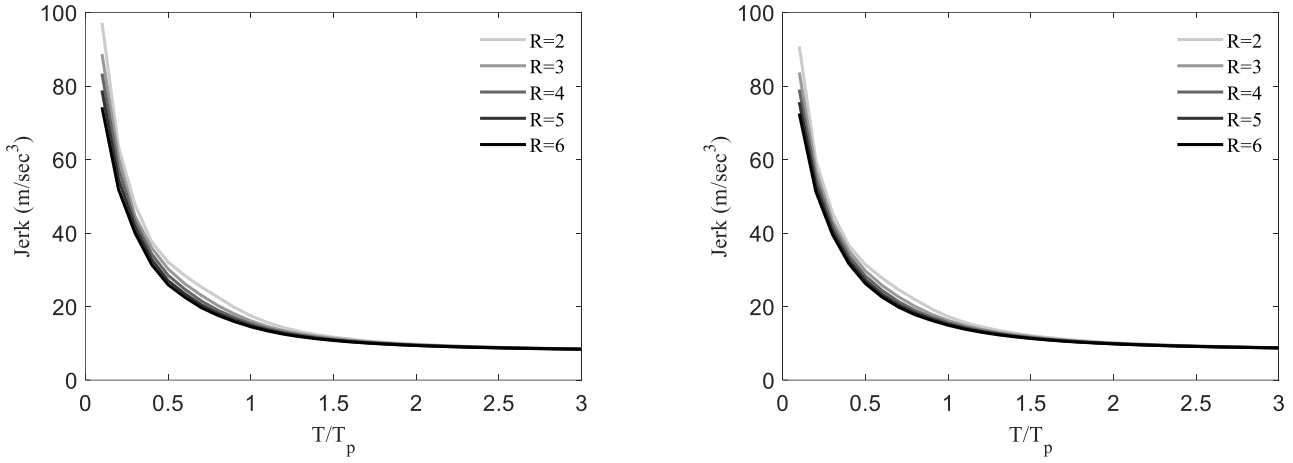

Fig. 2. Effect of the strength reduction factor on the mean jerk inelastic spectra for the PP hysteretic model with: (a): ξ = 0.05; (b): ξ = 0.10; (c): ξ = 0.15; (d): ξ = 0.20.

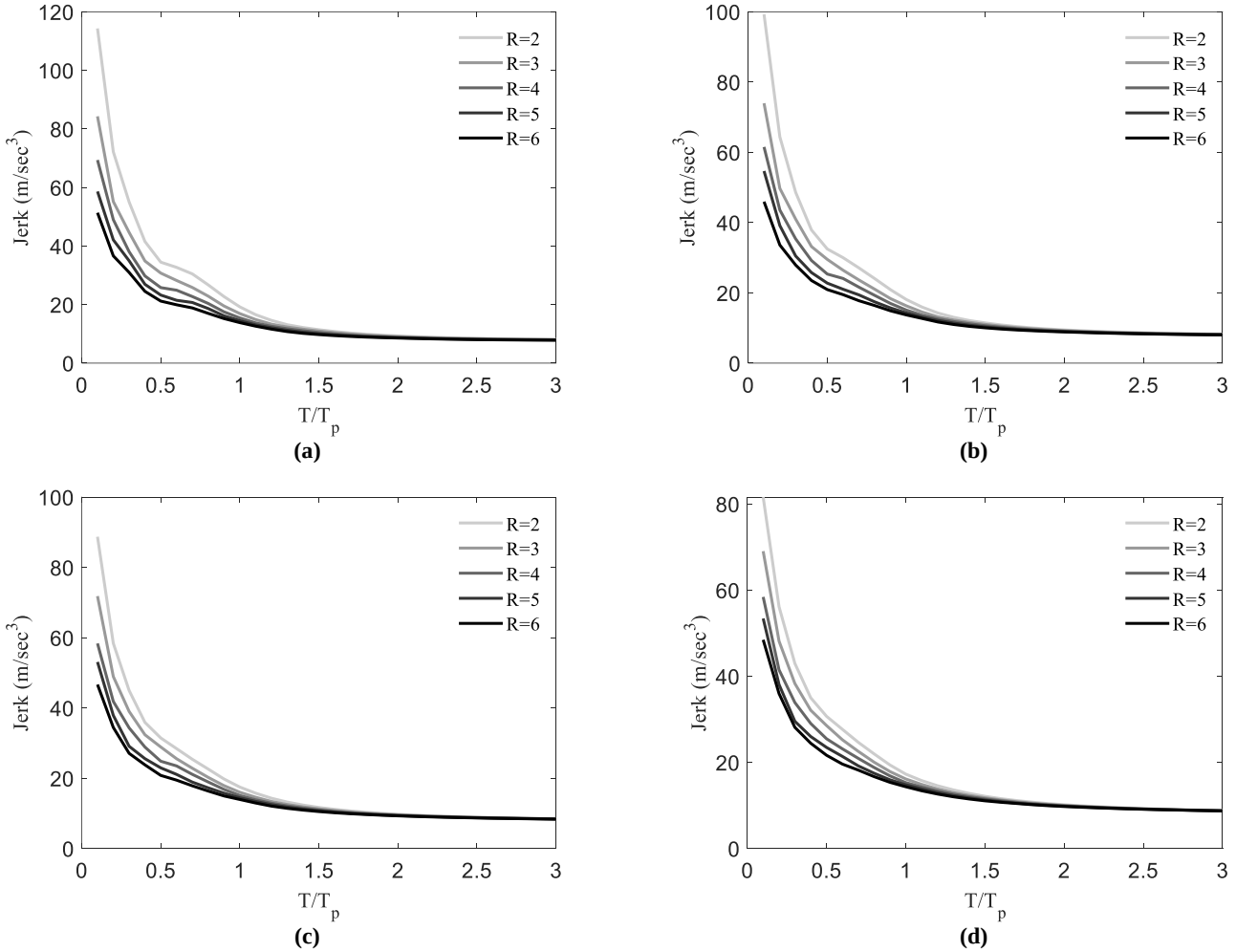

Fig. 3. Effect of the strength reduction factor on the mean jerk inelastic spectra for the DP hysteretic model with: (a): ξ = 0.05; (b): ξ = 0.10; (c): ξ = 0.15; (d): ξ = 0.20.

4.2. Effect of the viscous damping ratio on the inelastic jerk spectra

The effect of the viscous damping ratio on the mean jerk spectra is shown in Figs. 4 and 5 for the PP and DP behavior models, respectively. It is observed from Fig. 4 that this impact is slightly higher in the short normalized period region than in the long normalized period region. In other words, J values decline slightly if ξ increases. For instance, J varies from 35.77 m/s^3 to 31.40 m/s^3 for the SDOF systems with T/T_p = 0.5 and R = 2, when ξ changes from 0.05 to 0.2. Also, the effect of ξ on J becomes lower as R increases. On the other hand, the value of jerk remains stable in the long normalized period region. That is, if R = 2, and ξ = 0.05, J becomes constant by 9.13 m/s^3 on average in the period range $T/T_p \geq 1.5$. This grows slightly to 9.30 m/s^3, 9.54 m/s^3, 9.94 m/s^3 as ξ increases to 0.1, 0.15, and 0.2, respectively, for the same R.

Moreover, the sensitivity of J on ξ for the systems with short values of T/T_p decreases as R tends to increase, namely (R = 3, 4, 5, 6), however, the trend of the jerk response versus the damping ratio is similar as R = 2, as shown in Fig. 4(b)(c)(d)(e). Furthermore, similar trends can be concluded from Fig. 5 for the systems with the DP model, as discussed in Fig. 4; however, the value of the jerk parameter is lower for this type of behavior model.

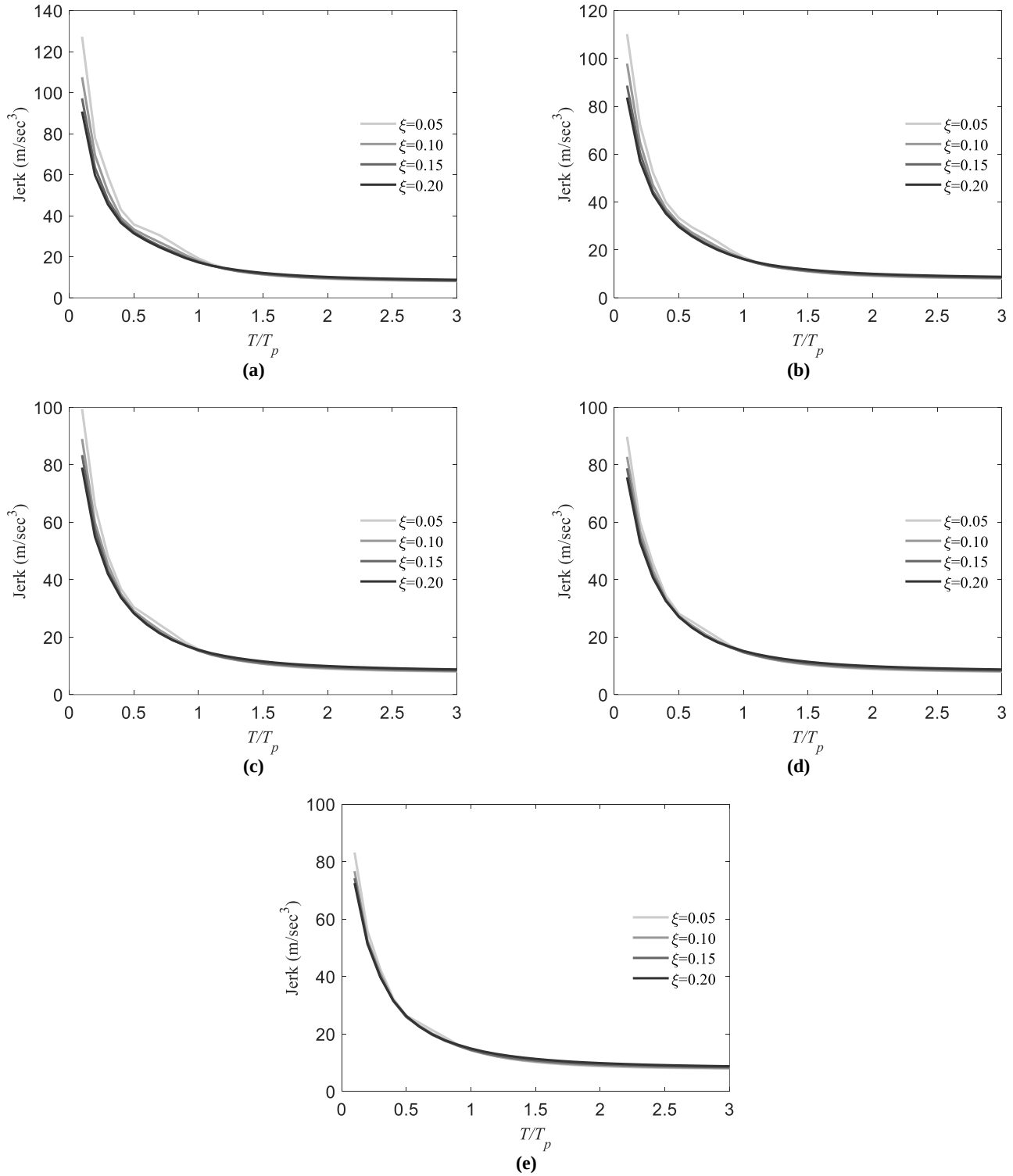

Fig. 4. Effect of the viscous damping ratio on the mean inelastic response spectra in terms of the jerk demand for the PP hysteretic rule and different strength reduction factors: (a) R = 2; (b) R = 3; (c) R = 4; (d) R = 5; and (e) R = 6.

4.3. Effect of the hysteretic model on the inelastic jerk spectra

Fig. 6 shows the sensitivity of the jerk response of the SDOF systems with R = 4 on the hysteretic models (PP and DP) for ξ = 0.05 and ξ = 0.10. As deduced from Fig. 6(a) that in the range of $T/T_p \leq$ 1.0 and ξ = 0.05, the jerk demand of the structures having the PP model is 23.94% on average higher than their equivalents having the DP model.

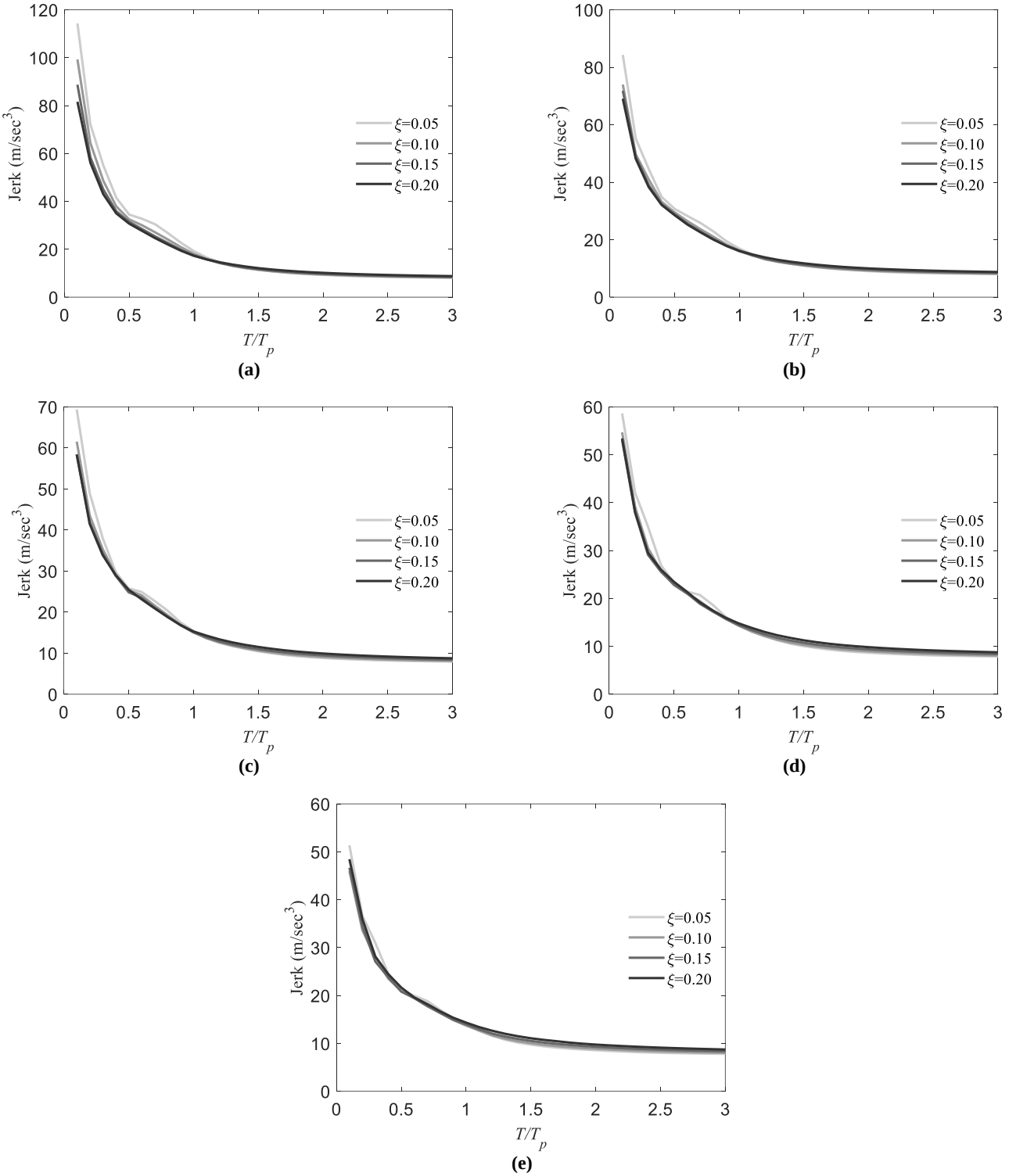

Fig. 5. Effect of the viscous damping ratio on the mean inelastic response spectra in terms of the jerk demand for the DP hysteretic rule and different strength reduction factors: (a) *R* = 2; (b) *R* = 3; (c) *R* = 4; (d) *R* = 5; and (e) *R* = 6.

This difference is negligible when $1.1 \leq T/T_p \leq 3.0$, such that this parameter remains constant in this range of T/T_p by 9.51 m/s^3 on average for both models. In addition, a comparative evaluation is depicted in Fig. 6(b) in the case of $\xi = 0.10$. It reveals that the systems with $T/T_p \leq 1.0$, ξ=0.10, and the PP model experience more jerk responses (22.84% on average) compared to those with the DP model. Furthermore, within the interval $1.1 \leq T/T_p \leq 3.0$, a stable level of the jerk parameter can be seen, whose average value is 9.68 m/s^3 for the two considered hysteretic models in the case of the DP model. This can arise from the fact that in long T/T_p ratios, structural response is governed by gradual displacement trends rather than sharp velocity shifts, which limits acceleration curvature and stabilizes jerk demand. It is noted that pinching and strength degradation reduce acceleration reversals and energy rebound, which directly suppresses jerk peaks, especially in the short T/T_p range.

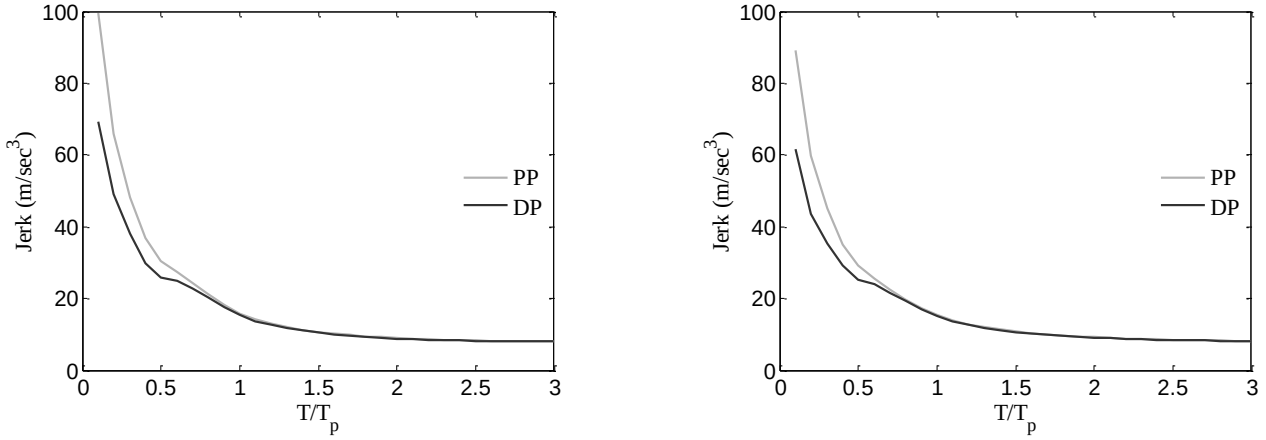

Fig. 6. Effect of the hysteretic model (PP and DP) on the mean inelastic response spectra in terms of the jerk demand for: (a) ξ = 0.05; (b) ξ = 0.1.

5. Prediction equation

In this section, an analytical equation is proposed to predict the mean jerk demand of the SDOF systems under the pulse-like earthquakes based on T/T_p and R for the two hysteretic models and the considered levels of ξ. Extensive nonlinear regression analyses are conducted employing the Least-Squares Fitting method based on the research results to find efficient models. Note that the equation can be extended to a class of steel or RC buildings for predicting the jerk response under pulse-like earthquakes. The mean values of the jerk demand (indicated by J) are predicted using Eq. 1. The unknown coefficient values (a1, a2, …, a8) for the PP and DP hysteretic models, as well as different levels of ξ considered in this study, are obtained from Table 4 and Table 5, respectively. The accuracy of the proposed equation is measured by the coefficient of determination, denoted as R^2. The R^2 values indicated in the tables reveal that the prediction equation is sufficiently accurate. Furthermore, Fig. 7 compares the mean values of jerk predicted by Eq. 1 for structures with the PP model and ξ = 0.05 with the actual values computed from nonlinear time history analyses. This comparison serves as an example of the additional verification and demonstrates the acceptable accuracy of the proposed equation. The presented equation can be employed to predict the jerk demand of structures based on their structural characteristics.

Eq. 1 is an empirical model fitted to the jerk responses obtained from 91 unscaled pulse-like ground motions. The predictor variables are the nondimensional period ratio T/T_p (with T_p the pulse period of each record) and the strength reduction factor R. Because the dataset includes records with a wide range of natural intensities and pulse characteristics, the effects of excitation amplitude are implicitly represented in the calibration through the resulting R values used in the regression. Therefore, Eq. 1 expresses the median relationship between absolute jerk demand, T/T_p, and R for the ensemble of records considered, rather than for any single motion. In practical use, the user applies Eq. 1 with the corresponding T_p of the selected record and the appropriate R value, provided these parameters lie within the calibration range of the 91 motions.

The relationship between jerk demand and structural damage can be interpreted through the strength reduction factor R, which reflects the ductility level of the system. As inelastic excursions increase (i.e., higher R), the system undergoes stiffness degradation and experiences a reduction in high-frequency response components. Consequently, the amplitude of the jerk response decreases with increasing R. This trend indicates that jerk can serve as a dynamic indicator of structural integrity, where large jerk spikes are associated with elastic or near-yield conditions, while reduced jerk amplitudes correspond to systems with pronounced inelastic behavior and energy dissipation.

$$J = a_1 + \frac{a_2}{T/T_p} + \frac{a_3}{R} + \frac{a_4}{\left(T/T_p\right)^2} + \frac{a_5}{R^2} + \frac{a_6}{(T/T_p)R} \quad (1)$$

Table 4. Values of unknown coefficients of Eq. 1 for the PP model.

ξ	a_1	a_2	a_3	a_4	a_5	a_6	R^2
0.05	-0.396	12.190	15.430	-0.611	-27.250	13.710	0.997
0.10	0.506	11.980	13.290	-0.589	-21.830	9.518	0.997
0.15	1.559	11.870	9.937	-0.572	-15.550	6.923	0.998
0.20	2.650	11.690	7.046	-0.562	-10.800	5.502	0.998

Table 5. Values of unknown coefficients of Eq. 1 for the DP model.

ξ	a_1	a_2	a_3	a_4	a_5	a_6	R^2
0.05	2.435	7.207	9.707	-0.588	-21.960	20.250	0.992
0.10	3.026	6.756	10.920	-0.542	-22.700	16.980	0.993
0.15	3.110	6.962	13.750	-0.510	-25.330	13.820	0.993
0.20	3.490	7.526	13.370	-0.510	-23.140	11.160	0.993

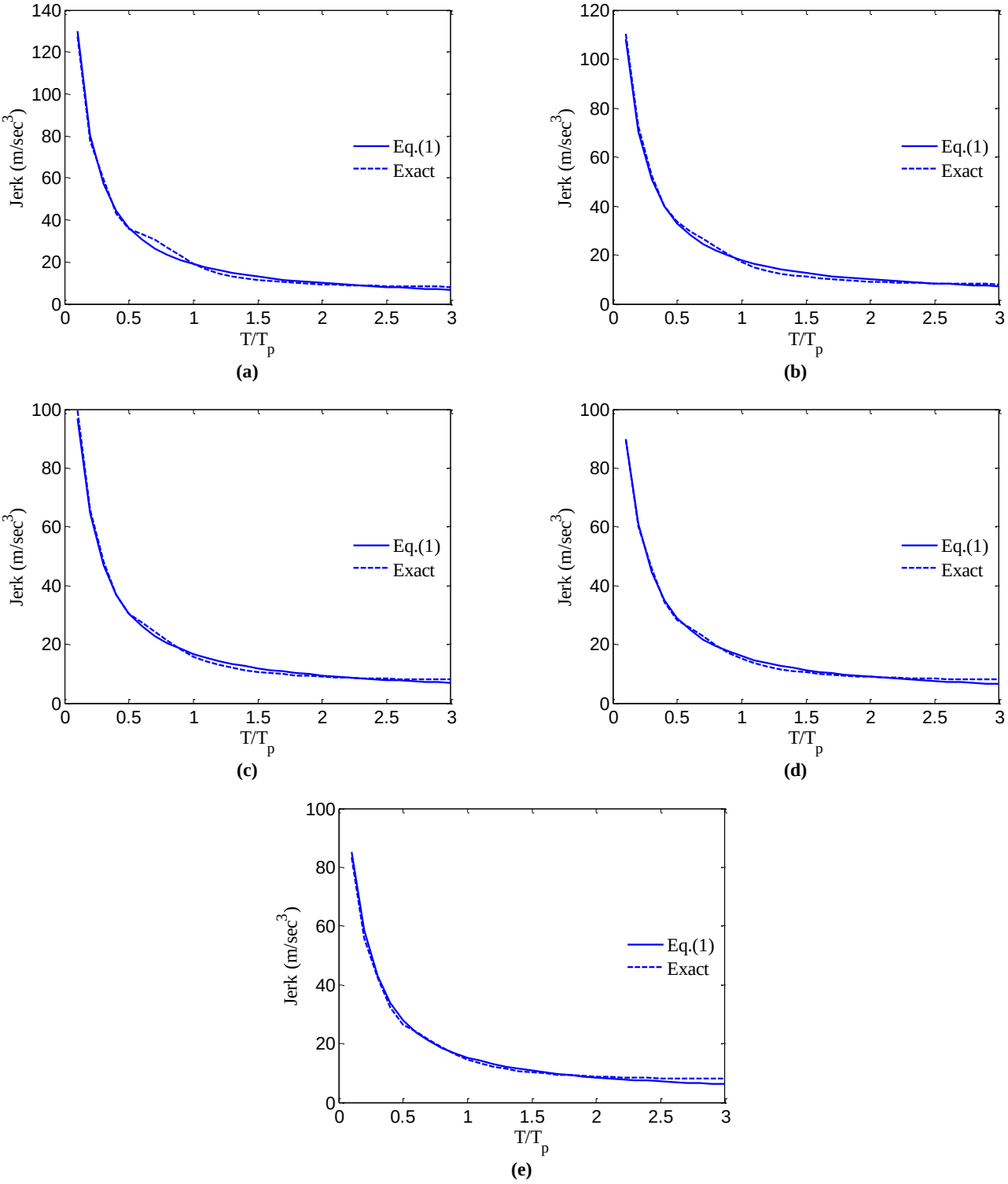

Fig. 7. Predicted values of jerk against actual ones for: (a) R = 2; (b) R = 3; (c) R = 4; (d) R = 5; and (e) R = 6.

6. Summary and conclusion

This study presents constant-strength spectra based on the jerk response of inelastic SDOF systems subjected to 91 pulse-like earthquakes. Different structural characteristics, including the strength reduction factor, hysteretic model, and viscous damping ratio, are considered. The key conclusions of this study are summarized as follows:

- The effect of R on the jerk demand of the structures with the PP model and $T/T_p \leq 1.0$ is relatively significant, such that this response increases as R decreases. For instance, the mean jerk of the SDOF system with $T/T_p = 0.5$ and $\xi = 0.05$ rises from 26.40 m/s^3 to 35.77 m/s^3 (an increase of about 35.5%) when R diminishes from 6 to 2. Moreover, in the range of $2.0 \leq T/T_p \leq 3.0$, the jerk response reaches a constant value of 8.40 m/s^3 on average for all the given R values.
- Similar trends can be observed for the DP model, such that for the same structure ($T/T_p = 0.5$ and $\xi = 0.05$), the mean jerk varies from 21.18 m/s^3 to 34.48 m/s^3 (an increase of roughly 62.80%), as R changes from 6 to 2.
- The effect of the viscous damping ratio on the jerk demand is slightly higher for the systems with short T/T_p values than for those with long values, such that J values decline slightly as ξ increases for the former structures. For example, as ξ changes from 0.05 to 0.2, the variation of J is from 35.77 m/s^3 to 31.40 m/s^3 for the SDOF systems with $T/T_p = 0.5$ and $R = 2$.
- In the long normalized period region ($T/T_p \geq 1.5$), with $R = 2$, and $\xi = 0.05$, the jerk parameter tends to stabilize at an average value of 9.13 m/s^3. This value rises marginally to 9.30 m/s^3, 9.54 m/s^3, and 9.94 m/s^3 as ξ increases to 0.1, 0.15, and 0.2, respectively, for the same R. Furthermore, the sensitivity of the jerk demand to ξ declines in the short normalized period region as R increases. However, the trend of J versus ξ is similar across all considered R values and for the DP model.
- For structures with $T/T_p \leq 1.0$ and $\xi = 0.05$, the jerk demand obtained using the PP model is, on average, 23.94% higher than that obtained using the DP model. This difference is negligible in the range of $1.1 \leq T/T_p \leq 3.0$, where the response is approximately constant at an average of 9.51 m/s^3 for both hysteretic models.
- A prediction equation is proposed to estimate the jerk demand of the structural systems as a function of the elastic vibration period normalized by the pulse period (T/T_p) and the strength reduction factor (R), considering different hysteretic models and viscous damping ratios.

Statements & Declarations

Author contributions

Alireza Garakaninezhad: Conceptualization, Methodology, Formal analysis, Investigation, Software, Validation, Visualization, Resources, Writing - Original Draft, Writing - Review & Editing.

Saeed Amiri: Conceptualization, Investigation, Resources, Writing - Review & Editing.

Funding

The authors received no financial support for the research, authorship, and/or publication of this article.

Data availability

The data presented in this study will be available on interested request from the corresponding author.

Declarations

The authors declare no conflict of interest.

References

[1] Hayati, H., Eager, D., Pendrill, A. M., Alberg, H. Jerk within the Context of Science and Engineering—A Systematic Review. Vibration, 2020; 3: 371-409. doi:10.3390/vibration3040025.

[2] Nemes, A., Mester, G. Energy Efficient Feasible Autonomous Multi-Rotor Unmanned Aerial Vehicles Trajectories. In: Proceedings of the 4th International Scientific Conference on Advances in Mechanical Engineering; 2016 Oct 15-16; Debrecen, Hungary. p. 369-376.

[3] Pendrill, A.-M. Rollercoaster loop shapes. Physics Education, 2005; 40: 517-521. doi:10.1088/0031-9120/40/6/001.

[4] Eager, D., Pendrill, A.-M., Reistad, N. Beyond velocity and acceleration: jerk, snap and higher derivatives. European Journal of Physics, 2016; 37: 065008. doi:10.1088/0143-0807/37/6/065008.

[5] Gierlak, P., Szybicki, D., Kurc, K., Burghardt, A., Wydrzyński, D., Sitek, R., Goczał, M. Design and dynamic testing of a roller coaster running wheel with a passive vibration damping system. Journal of Vibroengineering, 2018; 20: 1129–1143. doi:10.21595/jve.2017.18928.

[6] Sicat, S., Woodcock, K., Ferworn, A. Wearable technology for design and safety evaluation of rider acceleration exposure on aerial adventure attractions. In: Proceedings of the Annual Occupational Ergonomics and Safety Conference; 2018 Jun 7-8; Pittsburgh, Pennsylvania. p. 74-79.

[7] Vaisanen, A. Design of Roller Coasters (Master Thesis). Espoo (FI): Aalto University; 2018.

[8] Pendrill, A.-M., Eager, D. Velocity, acceleration, jerk, snap and vibration: forces in our bodies during a roller coaster ride. Physics Education, 2020; 55: 065012. doi:10.1088/1361-6552/aba732.

[9] Bae, I., Moon, J., Seo, J. Toward a Comfortable Driving Experience for a Self-Driving Shuttle Bus. Electronics, 2019; 8: 943. doi:10.3390/electronics8090943.

[10] Coats, T. W., Haupt, K. D., Murphy, H. P., Ganey, N. C., Riley, M. R. A Guide for Measuring, Analyzing, and Evaluating Accelerations Recorded During Seakeeping Trials of High-Speed Craft. Bethesda (MD): Naval Surface Warfare Center Carderock West Bethesda United States; 2016. Report No.: NSWCCD-80-TR-2016/003.

[11] Sosa, L., Ooms, J. A Comfort Analysis of an 86 m Yacht Fitted with Fin Stabilizers Vs. Magnus-Effect Rotors. In: 24th International HISWA Symposium on Yacht Design and Yacht Construction; 2016 Nov 14-15; Amsterdam, Netherlands. p. 1-13.

[12] Werkman, J. Determining and Predicting the Seakeeping Performance of Ships Based on Jerk in the Ship Motions (Master Thesis). Delft (NL): Delft University of Technology; 2019.

[13] Geoffrey Chase, J., Barroso, L. R., Hunt, S. Quadratic jerk regulation and the seismic control of civil structures. Earthquake Engineering & Structural Dynamics, 2003; 32: 2047-2062. doi:10.1002/eqe.314.

[14] He, Z., Xu, Y. Correlation between global damage and local damage of RC frame structures under strong earthquakes. Structural Control and Health Monitoring, 2017; 24: e1877. doi:10.1002/stc.1877.

[15] Taushanov, A. Jerk Response Spectrum. In: Proceedings of the International Jubilee Scientific Conference “75th Anniversary of UACEG”; 2017 Nov 1-3; Sofia, Bulgaria. p. 39-50.

[16] Tong, M., Wang, G.-Q., Lee, G. C. Time derivative of earthquake acceleration. Earthquake Engineering and Engineering Vibration, 2005; 4: 1-16. doi:10.1007/s11803-005-0019-6.

[17] Papandreou, I., Papagiannopoulos, G. On the jerk spectra of some inelastic systems subjected to seismic motions. Soil Dynamics and Earthquake Engineering, 2019; 126: 105807. doi:10.1016/j.soildyn.2019.105807.

[18] He, H., Li, R., Chen, K. Characteristics of jerk response spectra for elastic and inelastic systems. Shock and Vibration, 2015; 2015: doi:10.1155/2015/782748.

[19] Yaseen, A. A., Ahmed, M. S., Al-Kamaki, Y. S. S. The Possibility of Using Jerk Parameters as Seismic Intensity Measure. In: 3rd international conference on recent innovations in engineering (ICRIE); 2020 Sep 9-10; Duhok, Iraq. p. 254-277.

[20] Wakui, M., Iyama, J., Koyama, T. Estimation of plastic deformation of vibrational systems using the high-order time derivative of absolute acceleration. In: Proceedings of the 16th World Conference on Earthquake Engineering; 2017 Jan 9-13; Santiago, Chile. p. 3932.

[21] Vukobratović, V., Ruggieri, S. Jerk in earthquake engineering: State-of-the-art. Buildings, 2022; 12: 1123. doi:10.3390/buildings12081123.

[22] Amiri, S., Di Sarno, L., Garakaninezhad, A. On the aftershock polarity to assess residual displacement demands. Soil Dynamics and Earthquake Engineering, 2021; 150: 106932. doi:10.1016/j.soildyn.2021.106932.

[23] Amiri, S., Garakaninezhad, A., Bojórquez, E. Normalized residual displacement spectra for post-mainshock assessment of structures subjected to aftershocks. Earthquake Engineering and Engineering Vibration, 2021; 20: 403-421. doi:10.1007/s11803-021-2028-5.

[24] Amiri, S., Di Sarno, L., Garakaninezhad, A. Correlation between non-spectral and cumulative-based ground motion intensity measures and demands of structures under mainshock-aftershock seismic sequences considering the effects of incident angles. Structures, 2022; 46: 1209-1223. doi:10.1016/j.istruc.2022.10.076.

[25] Amiri, S., Koboevic, S. Inelastic spectra under mainshock-multiple aftershock sequences. In: 3rd European Conference on Earthquake Engineering & Seismology; 2022 Sep 4-9; Bucharest, Romania. p. 1-22.

[26] Garakaninezhad, A., Amiri, S., Noroozinejad Farsangi, E. Effects of Ground Motion Incident Angle on Inelastic Seismic Demands of Skewed Bridges Subjected to Mainshock–Aftershock Sequences. Practice Periodical on Structural Design and Construction, 2023; 28: 04023006. doi:10.1061/PPSCFX.SCENG-1218.

[27] Amiri, S., Koboevic, S. On the necessary number of aftershocks for seismic collapse risk assessment of buildings. In: 18th World Conference on Earthquake Engineering (WCEE2024); 2024 Jun 30-Jul 5; Milan, Italy. p. 1-9.

[28] Somerville, P. G., Smith, N. F., Graves, R. W., Abrahamson, N. A. Modification of Empirical Strong Ground Motion Attenuation Relations to Include the Amplitude and Duration Effects of Rupture Directivity. Seismological Research Letters, 1997; 68: 199-222. doi:10.1785/gssrl.68.1.199.

[29] Baker, J. W. Identification of near-fault velocity pulses and prediction of resulting response spectra. 1st ed. Reston (VA): 2008. doi:10.1061/40975(318)4.

[30] Rupakhety, R., Sigurdsson, S. U., Papageorgiou, A. S., Sigbjörnsson, R. Quantification of ground-motion parameters and response spectra in the near-fault region. Bulletin of Earthquake Engineering, 2011; 9: 893-930. doi:10.1007/s10518-011-9255-5.

[31] Ezzodin, A., Ghodrati Amiri, G., Raissi Dehkordi, M. A Random Vibration-Based Simulation Model for Nonlinear Seismic Assessment of Steel Structures Subjected to Fling-Step Ground Motion Records. Journal of Vibration Engineering & Technologies, 2022; 10: 2641-2655. doi:10.1007/s42417-022-00509-9.

[32] Bray, J. D., Rodriguez-Marek, A. Characterization of forward-directivity ground motions in the near-fault region. Soil Dynamics and Earthquake Engineering, 2004; 24: 815-828. doi:10.1016/j.soildyn.2004.05.001.

[33] Iervolino, I., Chioccarelli, E., Baltzopoulos, G. Inelastic displacement ratio of near-source pulse-like ground motions. Earthquake Engineering & Structural Dynamics, 2012; 41: 2351-2357. doi:10.1002/eqe.2167.

[34] Khoshnoudian, F., Ahmadi, E. Effects of pulse period of near-field ground motions on the seismic demands of soil–MDOF structure systems using mathematical pulse models. Earthquake Engineering & Structural Dynamics, 2013; 42: 1565-1582. doi:10.1002/eqe.2287.

[35] Khoshnoudian, F., Ahmadi, E. Effects of inertial soil–structure interaction on inelastic displacement ratios of SDOF oscillators subjected to pulse-like ground motions. Bulletin of Earthquake Engineering, 2015; 13: 1809-1833. doi:10.1007/s10518-014-9693-y.

[36] Baker, J. W. Quantitative Classification of Near-Fault Ground Motions Using Wavelet Analysis. Bulletin of the seismological society of America, 2007; 97: 1486-1501. doi:10.1785/0120060255.

[37] Zhai, C., Li, S., Xie, L., Sun, Y. Study on inelastic displacement ratio spectra for near-fault pulse-type ground motions. Earthquake Engineering and Engineering Vibration, 2007; 6: 351-355. doi:10.1007/s11803-007-0755-x.

[38] Dong, H., Han, Q., Du, X., Liu, J. Constant ductility inelastic displacement ratios for the design of self-centering structures with flag-shaped model subjected to pulse-type ground motions. Soil Dynamics and Earthquake Engineering, 2020; 133: 106143. doi:10.1016/j.soildyn.2020.106143.

[39] Ghanbari, B., Akhaveissy, A. H. Constant-damage residual ratios of SDOF systems subjected to pulse type ground motions. AUT Journal of Civil Engineering, 2020; 4: 145-154. doi:10.22060/ajce.2019.14984.5510.

[40] Dong, H., Han, Q., Qiu, C., Du, X., Liu, J. Residual displacement responses of structures subjected to near-fault pulse-like ground motions. Structure and Infrastructure Engineering, 2022; 18: 313-329. doi:10.1080/15732479.2020.1835997.

[41] Garakaninezhad, A., Amiri, S. Inelastic acceleration ratio of structures under pulse-like earthquake ground motions. Structures, 2022; 44: 1799-1810. doi:10.1016/j.istruc.2022.08.102.

[42] OpenSees Effects of Hysteretic-Material Parameters. 2006. Available online: https://opensees.berkeley.edu/OpenSees/manuals/usermanual/4052.htm (accessed on December 2025).

[43] Di Sarno, L., Amiri, S. Period elongation of deteriorating structures under mainshock-aftershock sequences. Engineering Structures, 2019; 196: 109341. doi:10.1016/j.engstruct.2019.109341.

[44] Mazzoni, S., McKenna, F., Scott, M. H., Fenves, G. L. OpenSees Command Language Manual. Pacific Earthquake Engineering Research (PEER) Center, 2006; 264: 137-158.

[45] Scott, M., Filippou, F. Hysteretic Material. 2016. Available online: https://opensees.berkeley.edu/wiki/index.php/Hysteretic_Material (accessed on December 2025).

[46] PEER ground motion database. Pacific Earthquake Engineering Research Center. 2010. Available online: https://ngawest2.berkeley.edu/ (accessed on December 2025).